HANSEN, N. K. & COPPENS, P. (1978). *Acta Cryst.* A**34**, 909–921.
HOLLADAY, A., LEUNG, P. & COPPENS, P. (1983). *Acta Cryst.* A**39**, 377–387.
NORTH, A. C. T., PHILLIPS, D. C. & MATHEWS, F. S. (1968). *Acta Cryst.* A**24**, 351–359.
STEVENS, E. D. & COPPENS, P. (1975). *Acta Cryst.* A**31**, 612–619.
STOUT, G. H. & JENSEN, L. H. (1968). *X-ray Structure Determination*, pp. 410–412. London: Macmillan.
STOUT, J. W. & REED, S. A. (1954). *J. Am. Chem. Soc.* **76**, 5279–5281.

Acta Cryst. (1993). B**49**, 599–604

Defect Structure and Diffuse Scattering of Zirconia Single Crystals Doped with 7 mol% CaO

BY TH. PROFFEN, R. B. NEDER AND F. FREY

Institut für Kristallographie und Mineralogie, Theresienstrasse 41, 8000 *München* 2, *Germany*

AND W. ASSMUS

Physikalisches Institut der Universität Frankfurt, Germany

(*Received* 21 *September* 1992; *accepted* 4 *January* 1993)

Abstract

The defect structure of 7 mol% calcium-stabilized zirconia (CSZ) is described in terms of a correlated distribution of microdomains within the cubic matrix of CSZ. It is shown that the defect structure is very similar to that of 15 mol% CSZ. The defect structure consists of two types of defects: microdomains based on a single oxygen vacancy with relaxed neighbouring ions and microdomains based on a pair of oxygen vacancies separated by $a3^{1/2}/2$ along $\langle 111 \rangle$. Calculations show that a tetragonal distortion cannot explain the observed diffuse scattering. Several arguments suggest that the defect structure is not that of the Φ_1 phase: first, the similarity of diffuse scattering of yttrium-stabilized zirconia, for which no Φ_1 phase exists; second, the diffuse scattering of CSZ is almost identical from 4 mol% CSZ up to 20 mol% CSZ; third, the diffuse scattering is temperature dependent; and fourth, a direct comparison of single-crystal intensities of the Φ_1 phase with the intensity of diffuse scattering.

Introduction

Pure cubic zirconia is thermodynamically stable only at temperatures above 2643 K. Below this temperature a tetragonal phase is stable down to 1200–1300 K. At room temperature a monoclinic phase is the stable polymorph. An average fluorite structure of zirconia can, however, be stabilized at room temperature by doping with oxides of various di- and trivalent metals such as Ca, Mg, Y and Yb. This cubic phase is stable over a range of compositions. The exact mechanism of the stabilization and the solution of the structure of the solid has been the scope of several investigations (Neder, Frey & Schulz, 1990*b*, and references therein). Neder *et al.* (1990*b*) showed that the disordered diffuse scattering of cubic zirconia stabilized by 15 mol% CaO (CSZ15) can be analyzed by the correlated distribution of microdomains* within a matrix of cubic zirconia.

There is, however, still a controversial debate concerning whether the diffuse scattering of calcium-stabilized zirconia (CSZ) may be analyzed equally well by microdomains within the Φ_1 structure (Rossell, Sellar & Wilson 1991; Rossell, 1992) or by locally ordered arrangements with tetragonal symmetry (Martin, Boysen & Frey, 1993; Andersen, Clausen, Hackett, Hayes, Hutchings, Macdonald & Osborn, 1986; Osborn, Andersen, Clausen, Hackett, Hayes, Hutchings & Macdonald, 1986). The relevant results obviously depend sensitively on the type of sample, *i.e.* single crystal or powder.

To clarify these points further, and to see how the defect structure changes with composition we have investigated the diffuse scattering of single crystals with 7 mol% CaO (CSZ7). The results should give an important insight into the stabilizing mechanism. Proffen, Neder, Frey, Keen & Zeyen (1993) deal with the temperature dependence of diffuse scattering in CSZ with different amounts of CaO.

* The terms 'domain' or 'microdomain' are used in this paper, because it is the usual terminology in this context. We are well aware that this terminology does not match the strict crystallographic definition of a domain.

Experimental

The CSZ7 samples used in this study were grown by the skull-melting technique. The size of the crystal used for the diffraction experiments was about 2 × 2 × 9 mm. The experiments were carried out at the neutron spectrometer MAN II at the FRM research reactor in Garching, Munich, Germany. The wavelength used was 1.093 Å. The $\lambda/2$ contamination was less than 0.1% and the observed intensity was corrected accordingly. Further experimental details are given by Neder *et al.* (1990*b*).

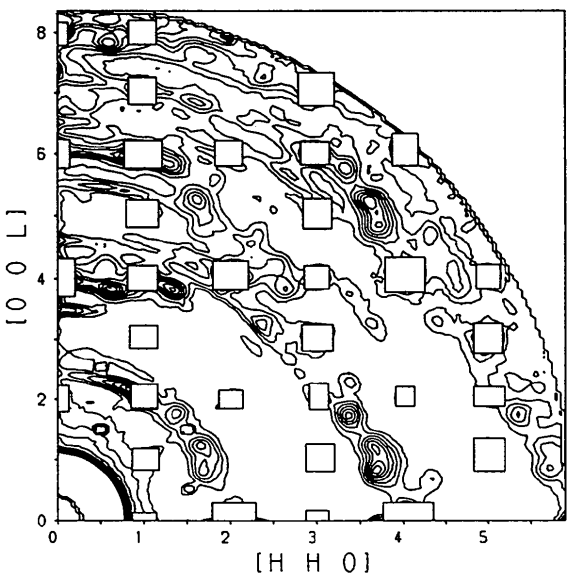

Fig. 1. Zero layer of the [1$\bar{1}$0] zone. The intensities are stepped with linear intervals of 25 counts, the lowest intensity represented is 125 counts.

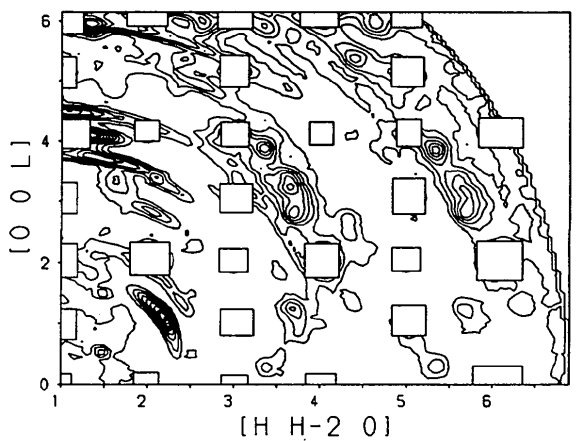

Fig. 2. Second layer of the [1$\bar{1}$0] zone. The intensities are stepped with linear intervals of 25 counts, the lowest intensity represented is 125 counts.

Measurements

The diffuse intensity was measured in two layers in the integral mode of the spectrometer, *i.e.* without analyzer crystal:

(I) $(hkl)[1\bar{1}0] = 0$ (Fig. 1);

(II) $(hkl)[1\bar{1}0] = 2$ (Fig. 2).

All layers were scanned in steps of 0.05 reciprocal-lattice constants in ⟨110⟩ and ⟨001⟩ directions.

In both layers of reciprocal space, Bragg reflections of the tetragonal as well as the cubic phases are observed. Diffuse maxima are observed that can be indexed as satellites with a satellite vector of $\pm(0.4\ 0.4 \pm 0.8)$. Visual inspection shows that the diffuse phenomena are very similar to those observed by Neder *et al.* (1990*b*) for CSZ15 and also similar to those observed for YSZ (Andersen, Clausen, Hackett, Hayes, Hutchings, Macdonald & Osborn, 1985; Osborn *et al.*, 1986). Broad bands of diffuse intensity are observed at higher $(\sin\theta)/\lambda$. Highly texturized powder rings are also visible.

Model and refinements

The theory of diffraction by correlated microdomains was presented by Neder, Frey & Schulz (1990*a*) and the model of a correlated distribution of microdomains was described in detail by Neder *et al.* (1990*b*). The same model was used in this study, since the diffuse phenomena appear to be reasonably similar. The microdomains are based on a single and a paired oxygen vacancy, respectively (Figs. 3, 4). In the microdomain based on a double vacancy the two vacancies are separated by $a3^{1/2}/2$ along ⟨111⟩ with a cation in between. The nearest neighbour oxygen ions around the vacancy are allowed to relax along ⟨100⟩ towards the vacancy. The cations are relaxed along ⟨111⟩. To maintain charge neutrality one of the cation neighbours is expected to be calcium.

The direction of the vector from the Ca ion to the oxygen vacancy is taken as the orientation of the microdomain. Eight different orientations result for the single-vacancy microdomain and four for the double-vacancy microdomain, since this microdomain has a centre of symmetry. The diffraction theory of Neder *et al.* (1990*a*) allows a description of the orientation that the first neighbouring microdomain can have with respect to a given microdomain. This correlation scheme is identical to the scheme that gave the best fit for CSZ15 in Neder *et al.* (1990*b*). The correlation scheme used restricts the orientations that two neighbouring single-vacancy microdomains can have with respect to each other. The orientation of the first neighbour has to be either parallel or at an angle of less than 54.7° to the orientation of a given single-vacancy microdomain. Thus, for a given single-vacancy microdomain of

orientation [111] the orientation of the first neighbouring microdomain can be: [111], [$\bar{1}$11], [1$\bar{1}$1], [11$\bar{1}$]. A double-vacancy microdomain can only be the first neighbour to a single vacancy if its orientation is parallel. The diameter of the double-vacancy microdomains is too large compared to the satellite vector to allow any correlation between two double-vacancy microdomains.

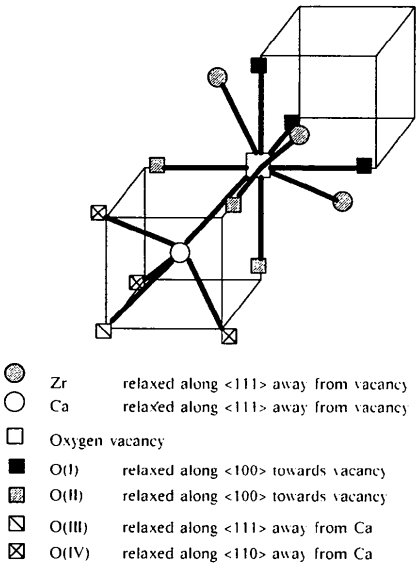

Fig. 3. Structure of the single-vacancy microdomain. The nearest neighbour ions are relaxed from their position in the ideal fluorite structure.

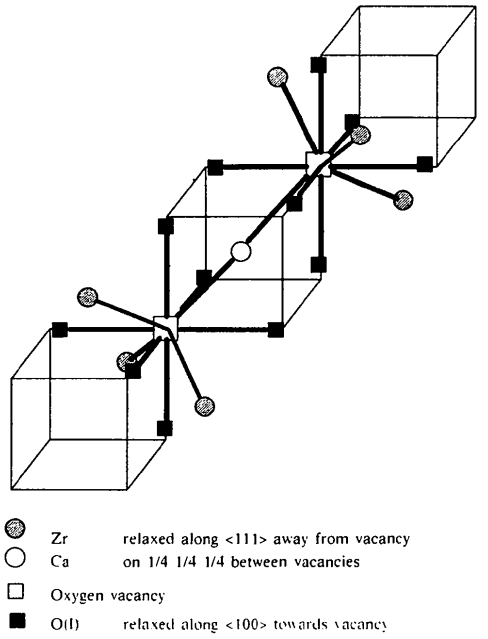

Fig. 4. Structure of the double-vacancy microdomain. The vacancies are separated by $a3^{1/2}/2$ along [111] with a cation in between. The nearest neighbour ions are relaxed from their position in the ideal fluorite structure.

As an alternative model for the microdomain the structure of tetragonal zirconia was used (Fig. 5). The occupation factors for the oxygen ions were adjusted to the vacancy rate in 7 mol% CSZ. No specific location was assumed for the oxygen vacancy for this microdomain. The oxygen ions were allowed to relax along ⟨001⟩. The ⟨001⟩ direction of the tetragonal cell was used as the orientation of the microdomain. Two schemes were used for the correlation. In the first scheme the next neighbour of a microdomain is restricted to the same orientation. In the second scheme any orientation is allowed for the next neighbour. For the sake of brevity these two schemes will be referred to as 'parallel' and 'all'.

The modulation indicated by the satellite vectors is about 5.2 Å. The lattice constants of the monoclinic Φ_1 phase (17.7, 14.5, 12.0 Å) are too large to use the structure of the Φ_1 phase as a microdomain.

For both of the models the calculated intensity was fitted to the observed intensities by least squares and a weighted residual R was calculated. The peak intensities of those points in reciprocal space corresponding to the satellite vectors were used as the data set for the fit. This resulted in a data set of 141 points. The following values were kept fixed: neutron wavelength 1.093 Å, relative abundance of Ca according to 7 mol% CaO; lattice constant 5.14 Å; neutron-scattering lengths, O 0.580, Zr 0.716, Ca 0.490 fm (Koester & Yelon, 1983); Debye–Waller factors, O 1.00, Zr 0.50, Ca 0.50 (Marxreiter, 1988, calculated by Rietveld refinements); discrete spacing of the microdomains [R_0 in equations (15) and (24) in Neder *et al.* (1990*a*)] $\frac{1}{2}d_{110}$, *i.e.* 3.6 Å.

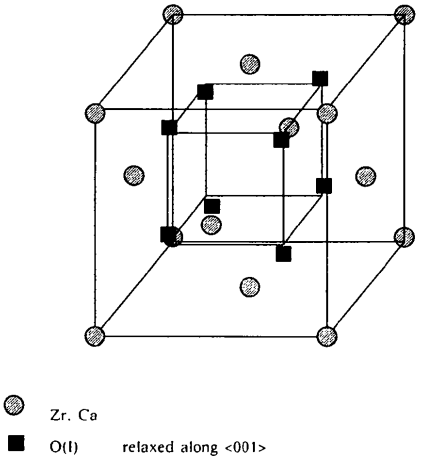

Fig. 5. Structure of the microdomain based on the structure of tetragonal zirconia. The oxygen ions are allowed to relax along [001].

The following parameters were refined:
(I) overall scale factor;
(II) one background parameter;
(III) positional parameters that describe the relaxation away from the positions in the ideal fluorite structure in the direction given by each model.
Model (I):
double-vacancy microdomain:
(*a*) oxygen relaxation in ⟨100⟩;
(*b*) cation relaxation in ⟨111⟩;
single-vacancy microdomain:
(*c*) O(I) relaxation in ⟨100⟩;
(*d*) O(II) relaxation in ⟨100⟩;
(*e*) O(III) relaxation in ⟨111⟩;
(*f*) O(IV) relaxation in ⟨110⟩;
(*g*) Zr relaxation in ⟨111⟩;
(*h*) Ca relaxation in ⟨111⟩.
Model (II):
(*a*) O relaxation in ⟨001⟩.

Results

The refinements of model (I) resulted in a weighted R value of 18.9% and goodness of fit of 2.4. The refined parameters are listed in Table 1. Figs. 6–9 show the calculated and difference intensities. Both layers show good correlation between the observed and calculated data. All diffuse peaks are present in the calculated intensity distributions and show the correct intensities to a good agreement. The powder rings were not included in the calculations and thus show in the difference intensity. The intensity of the broad bands is calculated too low, especially at high diffraction angles and the broadened shape of the diffuse peaks at (3.6, 3.6, 1.0), (1.6, 1.6, 1.0) and (5.6, 5.6, 3.0) is not reproduced by the calculations. The refinements of model (II) did not converge to a comparable agreement. The weighted R value was 29.9% for the correlation scheme 'parallel' and 30.8% for the correlation scheme 'all'. The calculated intensities do not match the observed intensities. The z parameter of the oxygen is not significantly shifted from 0.185, the position in the ideal tetragonal structure.

Table 1. *Relaxations away from the ideal fluorite positions of the atoms within the microdomains*

The left column gives the result of this work, the right column those of Neder *et al.* (1990*b*).

Parameter	Relaxation (Å)	Standard deviation	Relaxation (Å)	Standard deviation	
Single-vacancy microdomain					
O(1)	−0.11	±0.03	−0.06	±0.03	along ⟨100⟩
O(2)	0.11	±0.03	0.16	±0.03	along ⟨100⟩
O(3)	0.07	±0.02	0.12	±0.02	along ⟨111⟩
O(4)	0.09	±0.02	0.10	±0.02	along ⟨110⟩
Zr	0.13	±0.02	0.13	±0.02	along ⟨111⟩
Ca	0.23	±0.04	0.30	±0.05	along ⟨111⟩
Double-vacancy microdomain					
O	0.38	±0.03	0.41	±0.04	along ⟨100⟩
Zr	0.01	±0.03	0.12	±0.06	along ⟨111⟩

Discussion

The calculations show that the defect structure of CSZ7 stabilized zirconia is almost identical to the defect structure of 15 mol% CaO stabilized zirconia. It is characterized by two different microdomains that are coherently intergrown in the matrix of the disordered cubic crystal. The first microdomain is based on a single oxygen vacancy with relaxed next nearest neighbours. The second is based on two oxygen vacancies separated by $a3^{1/2}/2$ along [111]. In both compositions, the absolute value of the relaxation of nearest neighbouring ions is identical within the error limits. A microdomain based on the structure of tetragonal zirconia does not explain the observed diffuse intensity. Thus tetragonal distortions reported by Osborn *et al.* (1986) in yttrium-stabilized zirconia (YSZ) could not be confirmed for CSZ. This is further supported by the fact that YSZ shows a broad peak at (114) whereas CSZ does not show any marked diffuse scattering at (114) although Bragg reflections of the tetragonal phase are present in 7 mol% CSZ.

The defect structure of CSZ can therefore be interpreted as consisting of two areas. An area of correlated distributions of microdomains alternates with areas without correlated defects. In the second areas small defects are distributed at random. They give rise to the broad bands of diffuse scattering (Neder *et al.*, 1990*b*). The relative amount of these two areas changes as the composition of CSZ changes. The correlation of the microdomains and their internal structure remains unchanged. These findings of a crystal with a domain structure are supported by electron microscopic images of CSZ by Rossell *et al.* (1991).

Rossell *et al.* (1991), however, interpret the structure of the microdomains to be identical to that of the Φ_1 phase. Their interpretation is based on the fact that the contrast observed in electron microscope images is similar for the pure Φ_1 phase and for CSZ of 15–20 mol% CaO. This contrast is attributed to the ordering of the metal ions. Due to its weak scattering power for electrons, no direct information can be gained for oxygen.

We feel that several arguments support our model of the defect structure of CSZ. First, the diffuse scattering of YSZ, second the range of composition of CSZ throughout which the diffuse scattering can be observed, third the temperature dependence of the diffuse scattering of CSZ (*cf.* Proffen *et al.*, 1993), and fourth a direct comparison of diffuse intensity and Φ_1-phase single-crystal neutron diffraction data.

The diffuse scattering of YSZ (Andersen *et al.*, 1986; Osborn *et al.*, 1986) is very similar over a wide range of composition to that of CSZ. No structure similar to the Φ_1 phase exists, however, in the phase diagram of YSZ.

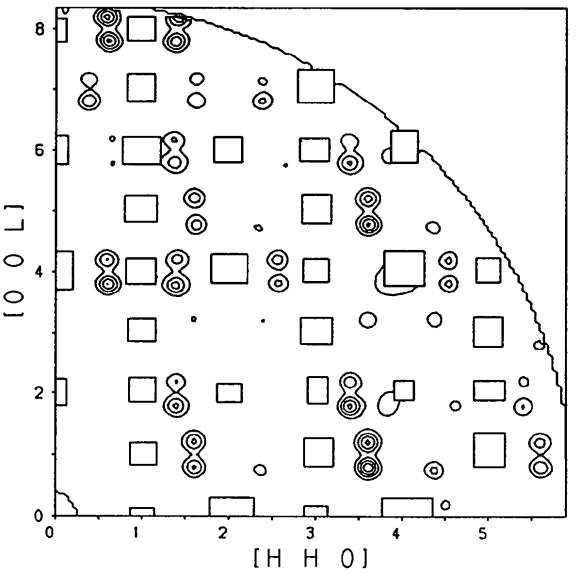

Fig. 6. Calculated intensity in the zero layer of the [1$\bar{1}$0] zone. The intensities are stepped with linear intervals of 25 counts, the lowest intensity represented is 125 counts. The Bragg reflections are represented by the rectangles.

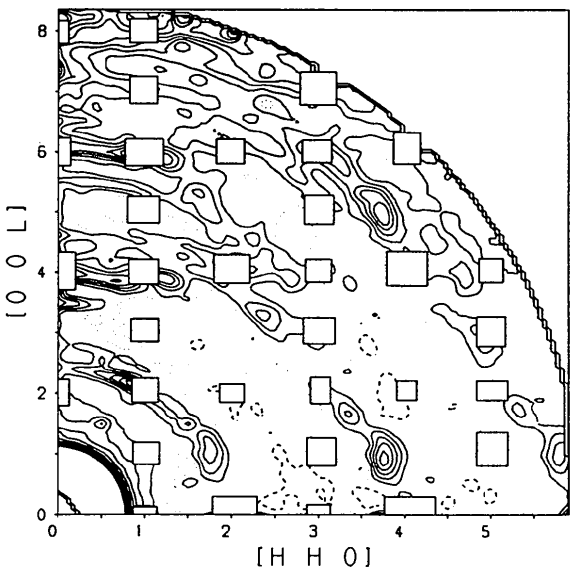

Fig. 7. Difference intensity $I_{obs} - I_{calc}$ in the zero layer of the [1$\bar{1}$0] zone. The intensities are stepped with linear intervals of 25 counts, the lowest intensity represented is 25 and -25 counts. Zero differences are represented by the dotted lines, negative intensities by the broken lines. The Bragg reflections are represented by the rectangles.

The diffuse scattering of CSZ has been shown in the literature to be extremely similar over a wide range of compositions. From 4 mol% CaO (Proffen, 1992) up to 20 mol% CaO diffuse maxima can be observed at identical positions in reciprocal space. Upon annealing at temperatures between 1450 and 1500 K in air for several months, samples with 15 to 20 mol% CaO will show sharp Bragg reflections of the Φ_1 phase (Hellmann & Stubican, 1983). Samples with less than 15 mol% CaO do not transform to the Φ_1 phase. If the structure of the microdomains in CSZ is that of the Φ_1 phase, similar transformations should be expected.

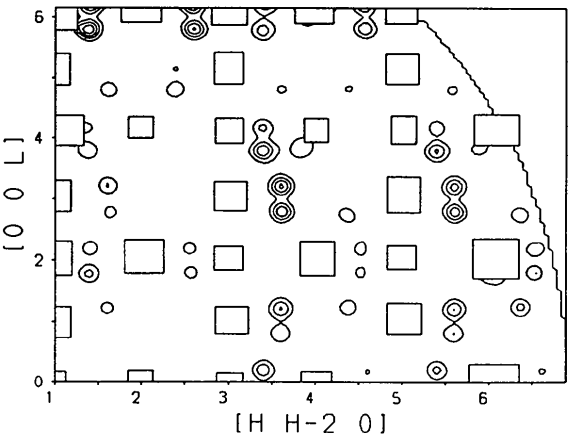

Fig. 8. Calculated intensity in the second layer of the [1$\bar{1}$0] zone. The intensities are stepped with linear intervals of 25 counts, the lowest intensity represented is 125 counts. The Bragg reflections are represented by the rectangles.

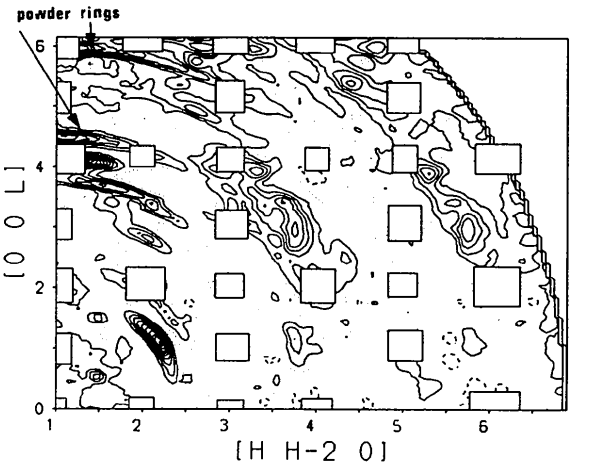

Fig. 9. Difference intensity $I_{obs} - I_{calc}$ in the second layer of the [1$\bar{1}$0] zone. The intensities are stepped with linear intervals of 25 counts, the lowest intensity represented is 25 and -25 counts. Zero differences are represented by the dotted lines, negative intensities by the broken lines. The Bragg reflections are represented by the rectangles.

Table 2. *Comparison of the measured diffuse intensity and the measured intensity of the Φ_1 phase reflections*

Fluorite indices			Φ_1 indices			Intensity		
						Diffuse	Φ_1	Difference
1.40	1.40	0.20	6	0	−4	82	1673	−1591
0.20	0.20	0.40	2	0	2	79	172	−93
1.20	1.20	0.40	−4	0	4	55	44	11
1.80	1.80	1.40	10	0	−4	101	101	0
0.80	0.80	1.60	0	0	4	75	191	−116
0.60	0.60	1.80	6	0	0	114	783	−669
0.60	0.60	1.80	6	0	0	114	866	−752
0.60	0.60	2.20	2	0	4	74	429	−355
1.40	−0.60	0.20	2	−4	−1	87	2989	−2902
1.60	−0.40	0.20	−2	4	2	80	19	61
1.60	−0.40	0.20	−2	4	2	80	23	57
1.60	−0.40	0.20	−2	4	2	80	55	25
1.60	−0.40	0.20	−2	4	2	80	6	74
1.60	−0.40	0.20	−2	4	2	80	9	71
2.40	0.4	0.20	6	−4	−4	274	217	57
2.60	0.60	0.20	−6	4	5	80	5687	−5607
2.60	0.60	0.20	−6	4	5	80	5560	−5480
1.80	−0.20	0.60	−2	4	3	58	77	−19
2.20	0.20	0.60	−6	4	3	57	49	8
1.20	−0.80	0.40	0	4	1	86	23	63
1.20	−0.80	0.40	0	4	1	86	3	83
1.80	−0.20	0.40	4	−4	−2	67	57	10
2.20	0.20	0.40	−4	4	4	106	24	82
1.40	−0.60	0.80	0	4	2	56	78	−22
1.60	−0.40	0.80	4	−4	−1	104	52	52
1.60	−0.40	0.80	4	−4	−1	104	119	−15
2.40	0.40	0.80	−4	4	5	56	179	−123
2.40	0.40	0.80	−4	4	5	56	249	−193
2.60	0.60	0.80	8	−4	−4	199	50	149
2.60	0.60	0.80	8	−4	−4	199	3	196
1.60	−0.40	1.20	0	4	3	100	2463	−2363
1.20	−0.80	1.40	2	4	2	36	13	23
1.80	−0.20	1.40	6	−4	−1	44	36	8
2.40	0.40	1.20	8	−4	−3	112	5024	−4912
2.20	0.20	1.40	−2	4	5	49	140	−91
1.80	−0.20	1.60	0	4	4	68	21	47

The temperature dependency of the diffuse scattering of CSZ will be described in detail by Proffen *et al.* (1993). We observed that the intensity of the diffuse scattering remains almost constant up to temperatures of about 1150 K. At 1350 K the intensity is reduced to less than one third. From 1350 up to 1750 K it remains almost constant again. Over the whole temperature range the full width at half maximum (FWHM) stays constant. This process is reversible, as was shown for 15 mol% CSZ by Neder *et al.* (1990*b*). The correlation among the defects remains basically the same over the whole temperature range. Between 1150 and 1350 K the relative volume of correlated defects decreases dramatically. Contradictory to this decrease in volume fraction, the Φ_1 phase, however, is stable from 1450 to 1500 K (Hellmann & Stubican, 1983). During the crystallization of single crystals of CSZ the crystals are cooled from the melt to room temperature within a few days. This time is too short to allow for cation order which plays a significant role in the structure of the Φ_1 phase.

Upon annealing a single crystal of 15 mol% CSZ for 3 months at 1450 K in air, a large volume fraction of the single crystal is transformed into the Φ_1 phase. The intensities of Φ_1-phase reflections were measured by neutron diffraction using instrument D19 at the ILL, Grenoble. Table 2 lists those reflections that lie in the zero and in the second layer of the $[1\bar{1}0]$ zone. The table also lists the intensity of the diffuse scattering of 15 mol% CaO as measured by Neder *et al.* (1990*b*). The intensities have been scaled so that the intensity of the Φ_1-phase reflection $10\,0\,\bar{4}$ and the corresponding fluorite intensity at 1.8 1.8 1.4 are equal. The table shows that the two sets of intensities – measured diffuse intensity and measured Φ_1-phase intensities – do not match.

As described by Allpress & Rossell (1975) and by Marxreiter, Boysen, Frey, Schulz & Vogt (1990), the basic building block of the Φ_1 phase that distinguishes this phase from the ideal fluorite phase, is a pair of oxygen vacancies that are separated by $3^{1/2}/2$ of the basic fluorite subcell with a cation in between the vacancies. This vacancy arrangement corresponds to the double-vacancy microdomain in our model. In other words, a basic structure element of the Φ_1 phase is one structure element in the microdomain description as used here.

This work was supported by funds of the BMFT (grant No. 03-SC2LMU).

References

ALLPRESS, J. G. & ROSSELL, H. J. (1975). *J. Solid State Chem.* **15**, 68–78.

ANDERSEN, N. H., CLAUSEN, K., HACKETT, M. A., HAYES, W., HUTCHINGS, M. T., MACDONALD, J. E. & OSBORN, R. (1985). *Proceedings of the 6th Risø International Symposium on Metallurgy and Materials Science*, edited by F. W. POULSEN, N. H. ANDERSEN, K. CLAUSEN, S. SKAARUP & O. T. SORENSEN, pp. 279–284. London: Institution of Mining and Metallurgy.

ANDERSEN, N. H., CLAUSEN, K., HACKETT, M. A., HAYES, W., HUTCHINGS, M. T., MACDONALD, J. E. & OSBORN, R. (1986). *Physica (Utrecht)*, **136B**, 315–317.

HELLMANN, J. R. & STUBICAN, V. S. (1983). *J. Am. Ceram. Soc.* **66**, 260–264.

KOESTER, L. & YELON, B. (1983). Neutron Diffraction Newsletter.

MARTIN, U., BOYSEN, H. & FREY, F. (1993). *Acta Cryst.* B**49**, 403–413.

MARXREITER, J. (1988). Personal communication.

MARXREITER, J., BOYSEN, H., FREY, F., SCHULZ, H. & VOGT, T. (1990). *Mater. Res. Bull.* **25**, 435–442.

NEDER, R. B., FREY, F. & SCHULZ, H. (1990*a*). *Acta Cryst.* A**46**, 792–798.

NEDER, R. B., FREY, F. & SCHULZ, H. (1990*b*). *Acta Cryst.* A**46**, 799–809.

OSBORN, R., ANDERSEN, N. H., CLAUSEN, K., HACKETT, M. A., HAYES, W., HUTCHINGS, M. T. & MACDONALD, J. E. (1986). *Mater. Sci. Forum.* **7**, 55–62.

PROFFEN, TH. (1992). Unpublished work.

PROFFEN, TH., NEDER, R. B., FREY, F., KEEN, D. A. & ZEYEN, C. M. E. (1993). *Acta Cryst.* B**49**, 605–610.

ROSSELL, H. J. (1992). Personal communication.

ROSSELL, H. J., SELLAR, J. R. & WILSON, I. J. (1991). *Acta Cryst.* B**47**, 862–870.